Supplementary Materials

Chirality, gelation ability and crystal structure: together or apart? Alkyl phenyl ethers of glycerol as simple LMWGs

Alexander A. Bredikhin,* Aidar T. Gubaidullin, Zemfira A. Bredikhina, Robert R. Fayzullin and Olga A. Lodochnikova

Arbuzov Institute of Organic and Physical Chemistry, FRC Kazan Scientific Center of RAS, Arbuzov St., 8, Kazan 420088, Russian Federation; aidar@iopc.ru (A.T.G.); zemfira@iopc.ru (Z.A.B.); fayzullin@iopc.ru (R.R.F.); olga@iopc.ru (O.A.L);

* Correspondence: baa@iopc.ru (A.A.B.)

The chemical structures and numbering of the investigated compounds.

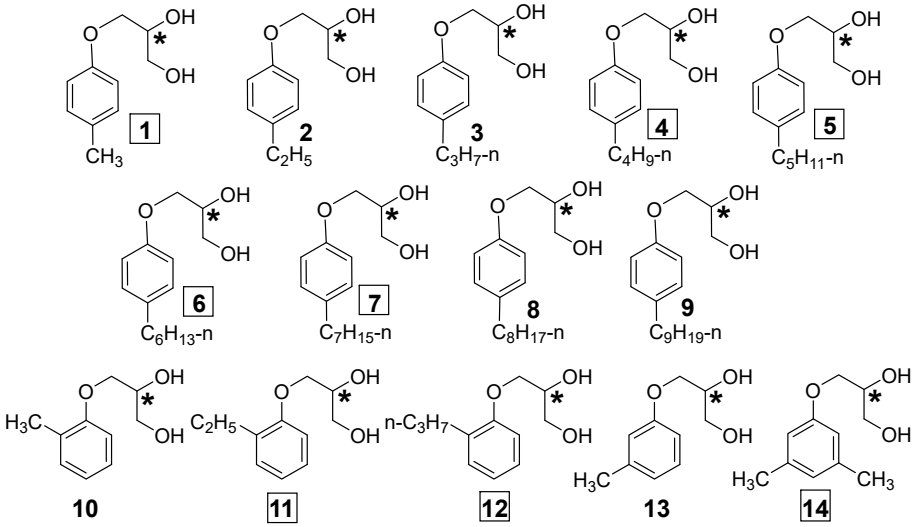

Table S1. Specific rotation of gels formed by compounds **1**, **11** and **14** in nonane[1].

Lines	Comp.	*Ee*, %	Conc., mmol L^{-1}	*c*, g/100 ml	$[\alpha]_D^{20}$	$[\alpha]_{578}^{20}$	$[\alpha]_{546}^{20}$	$[\alpha]_{436}^{20}$	$[\alpha]_{365}^{20}$
1	(*S*)-**1**	96	4.3	0.078	-147	-147	-180	-310	-662
2	(*S*)-**1**[2]	96	4.3	0.078	-268	-288	-325	-460	-768
3	(*R*)-**1**	90	3.5	0.064	+94	+94	+104	+175	+290
4	(*S*)-**11**	99	11.2	0.22	-270	-312	-380	-713	-1350
5	(*R*)-**11**	99.9	10.8	0.21	+287	+298	+349	+659	+1187
6	(*S*)-**14**	99	7.0	0.12	-59	-61	-73	-138	-253
7	(*R*)-**14**	99.9	6.8	0.13	+58	+61	+71	+158	+302

[1].- The gel formation occurred when the indicated solutions were cooled from 50 to 20 °C at a rate of degrees per minute; $[\alpha]_\lambda = \alpha/c \cdot l$, where α – optical rotation (deg), *c* – concentration (g/100 mL), *l* – cell length (dm).
[2].- The gel was aged at r.t. in a glass cell over night.

Table S2. Summary of crystal data and structure refinement details for (*R*)-**5**-**9** and *rac*-**14** compounds.

Compound	(*R*)-**5**	(*R*)-**6**	(*R*)-**7**	(*R*)-**8**	(*R*)-**9**	*rac*-**14**
Empirical formula	$C_{14}H_{22}O_3$	$C_{15}H_{24}O_3$	$C_{16}H_{26}O_3$	$C_{17}H_{28}O_3$	$C_{18}H_{30}O_3$	$C_{11}H_{16}O_3$
Formula weight	238.31	252.34	266.37	280.39	294.42	196.24
Temperature (K)	293(2)	293(2)	293(2)	293(2)	293(2)	296(2)
Radiation, wavelength (Å)	Mo *Kα*, 0.71073	Mo *Kα*, 0.71073	Mo *Kα*, 0.71073	Mo *Kα*, 0.71073	Mo *Kα*, 0.71073	Mo *Kα*, 0.71073
Crystal system	Orthorhombic	Monoclinic	Orthorhombic	Monoclinic	Monoclinic	Triclinic
Space group	$P2_12_12_1$ (No. 19)	$I2$ (No. 5)	$P2_12_12_1$ (No. 19)	$P2_1$ (No. 4)	$P2_1$ (No. 4)	*P-1* (No. 2)
Unit cell dimensions (Å; deg)	a = 4.886(3), b = 7.523(4), c = 37.99(2)	a = 9.884(4), b = 4.6635(17), c = 64.54(2); β = 94.057(9)	a = 4.913(3), b = 7.353(5), c = 44.59(3)	a = 9.870(3), b = 4.6213(15), c = 36.518(12); β = 90.947(4)	a = 8.677(4), b = 5.655(3), c = 36.618(17); β = 96.376(6)	a =5.2855(12), b = 9.140(2), c = 11.807(3), α= 71.003(15), β = 80.330(15), γ = 89.103(15)
Volume (Å^3)	1396.2(12)	2967.3(19)	1611(2)	1665.4(9)	1785.5(15)	531.2(2)
Z and Z'	4 and 1	8 and 2	4 and 1	4 and 2	4 and 2	2 and 1
Calculated density (g cm^{-3})	1.134	1.130	1.099	1.118	1.095	1.227
Packing index (%)	64.5	64.8	63.7	65.2	64.5	67.7
Absorption coefficient (mm^{-1})	0.078	0.077	0.074	0.075	0.072	0.088
F(000)	520	1104	584	616	648	212
θ range for data collection	2.144 to 25.311°	1.898 to 25.250°	2.808 to 25.239°	1.673° to 25.183°	1.679° to 25.250°	1.85° to 32.574°
Index ranges	$-5 \le h \le 5$, $-9 \le k \le 8$,	$-8 \le h \le 11$, $-5 \le k \le 5$,	$-5 \le h \le 5$, $-8 \le k \le 8$,	$-11 \le h \le 11$, $-5 \le k \le 5$,	$-10 \le h \le 10$, $-6 \le k \le 6$,	$-7 \le h \le 7$, $-13 \le k \le 13$,

	$-45 \le l \le 45$	$-76 \le l \le 77$	$-53 \le l \le 52$	$-43 \le l \le 43$	$-43 \le l \le 43$	$-17 \le l \le 17$
Reflections collected	10353	8119	10888	11924	33347	12065
Independent reflections	2510	4625	2901	5897	6459	3739
R_{int}	0.0559	0.0611	0.0817	0.0262	0.0638	0.0416
R_{σ}	0.0498	0.1325	0.0846	0.0425	0.0413	0.0438
Observed Data [$I > 2\sigma(I)$]	1625	2312	1727	4186	5443	2052
Completeness to θ_{max} (%)	99.4	99.5	99.7	99.6	99.9	99.1
Absorption correction	Numerical	Numerical	Numerical	Numerical	Numerical	Multi-scan
Max. and min. transmission	0.9705 and 0.8731	0.8620 and 0.7059	0.9580 and 0.6700	0.9580 and 0.8263	0.9705 and 0.6457	0.9345 and 0.9928
Data / restraints / parameters	2510 / 1 / 164	4625 / 2 / 332	2901 / 380 / 257	5897 / 7 / 379	6459 / 5 / 397	3739 / 0 / 135
Goodness-of-fit on F^2	1.021	1.034	1.067	1.044	1.038	1.017
Final R indices [$I > 2\sigma(I)$]	$R1 = 0.0446$, $wR2 = 0.0976$	$R1 = 0.0867$, $wR2 = 0.2024$	$R1 = 0.0798$, $wR2 = 0.1930$	$R1 = 0.0457$, $wR2 = 0.1027$	$R1 = 0.0540$, $wR2 = 0.1439$	*R1 = 0.0521, wR2 = 0.1437*
R indices (all data)	$R1 = 0.0797$, $wR2 = 0.1131$	$R1 = 0.1809$, $wR2 = 0.2573$	$R1 = 0.1281$, $wR2 = 0.2158$	$R1 = 0.0714$, $wR2 = 0.1160$	$R1 = 0.0638$, $wR2 = 0.1512$	*R1 = 0.1039, wR2 = 0.1768*
Largest diff. peak and hole (e Å^{-3})	0.114 and –0.106	0.394 and –0.354	0.145 and –0.166	0.103 and –0.138	0.172 and –0.179	0.217 and -0.197

Table S3. Selected torsion angles for glycerol moiety of the molecules (*R*)-**5-9** in the crystals.

Molecule	Torsion angle, deg				
	O1–C1–C2–C3	O1–C1–C2–O2	C1–C2–C3–O3	C2–C3–O3–C4	C3–O3–C4–C5
(*R*)-**5**	52.7(3)	–67.0(3)	55.9(3)	176.3(3)	3.3(4)
(*R*)-**6A**	–160.0(7)	73.3(9)	–58.2(10)	–179.7(7)	0.4(11)
(*R*)-**6B**	175.1(7)	59.2(8)	64.8(8)	177.4(6)	–0.2(11)
(*R*)-**7**	52.2(7)	–69.0(6)	54.8(6)	177.1(5)	2.2(8)
(*R*)-**8A**	–158.6(3)	77.1(3)	–54.4(4)	179.2(3)	–2.2(4)
(*R*)-**8B**	174.8(3)	57.8(3)	62.0(3)	178.5(2)	1.8(4)
(*R*)-**9A**	173.2(3)	53.3(4)	174.8(3)	170.6(2)	–169.8(3)
(*R*)-**9B**	–177.6(3)	59.9(3)	–58.2(3)	–166.4(2)	166.5(3)

Table S4. Main geometrical parameters of classical hydrogen bonds in the crystals (*R*)-**5-9**.

Compound	Interaction O–H···O'	Interatomic distances (Å)			Angle O–H···O' (deg)	Symmetry operation
		d(O–H)	d(H···O')	d(O···O')		
(*R*)-**5**	O1–H1···O2	0.82(3)	1.88(3)	2.699(3)	172(4)	2–*x*, *y*+0.5, 1.5–*z*
	O2–H2···O1	0.82(3)	1.88(3)	2.691(4)	175(3)	*x*+1, *y*, *z*
(*R*)-**6**	O1A–H1A···O2A	0.82	1.98	2.784(9)	166.1	*x*, *y*+1, *z*
	O2A–H2A···O2B	0.82	2.08	2.882(7)	164.5	1.5–*x*, *y*–0.5, 0.5–*z*
	O1B–H1B···O1B	0.82	1.93	2.746(6)	170.2	0.5–*x*, *y*–0.5, 0.5–*z*
	O2B–H2B···O1A	0.82	1.89	2.671(8)	159.5	n/a
(*R*)-**7**	O1–H1···O2	0.817(14)	1.88(2)	2.683(6)	167(8)	–*x*, *y*–0.5, 1.5–*z*
	O2–H2···O1	0.824(14)	1.871(19)	2.688(6)	171(7)	*x*–1, *y*, *z*
(*R*)-**8**	O1A–H1A···O2A	0.83(3)	1.94(3)	2.749(4)	166(4)	*x*, *y*–1, *z*
	O2A–H2A···O2B	0.82(3)	2.08(3)	2.870(3)	162(4)	1–*x*, *y*+0.5, 1–*z*
	O1B–H1B···O1B	0.83(3)	1.90(3)	2.723(2)	172(5)	–*x*, *y*+0.5, 1–*z*
	O2B–H2B···O1A	0.84(3)	1.87(3)	2.684(3)	162(4)	n/a
(*R*)-**9**	O1A–H1A···O1B	0.827(13)	1.939(17)	2.749(4)	166(4)	n/a
	O2A–H2A···O1A	0.812(13)	1.895(17)	2.682(3)	163(4)	1–*x*, *y*–0.5, 1–*z*
	O1B–H1B···O2A	0.820(14)	1.954(18)	2.761(4)	168(5)	1–*x*, *y*–0.5, 1–*z*
	O2B–H2B···O2A	0.824(14)	2.35(3)	3.031(4)	140(4)	1–*x*, *y*+0.5, 1–*z*
	O2B–H2B···O3A	0.824(14)	2.17(3)	2.879(3)	144(4)	1–*x*, *y*+0.5, 1–*z*

Powder XRD results for compound (R)-4.

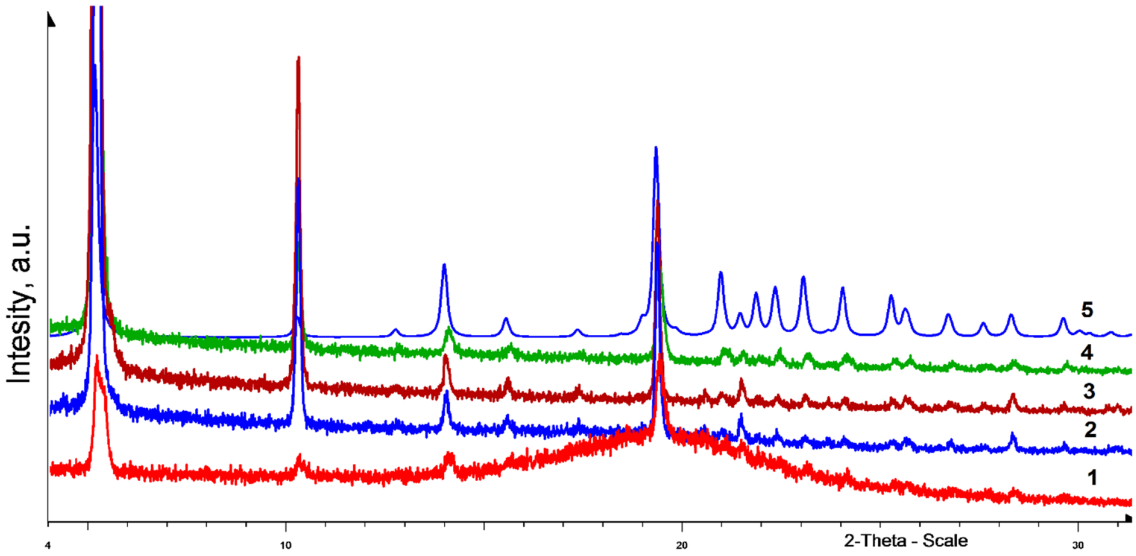

Figure S1. Powder diffraction patterns (bottom-up): (1–4) evolution of the diffraction of a gel based on (*R*)-**4** as the solvent naturally evaporates; (5) theoretical diffraction pattern calculated from single crystal data for (*R*)-**4** diol. For clarity, the curves are vertically shifted relative to each other along the intensity axis.

The gel formed in the (*R*)-**4**/nonane system is weak and not very stable. Therefore, already in the initial diffractogram of the gel (Figure S1, curve 1), in addition to the amorphous halo, diffraction peaks are observed in the range of scattering angles 5, 10, 14, and 19-20°, which indicates the presence of a crystalline phase in the sample. As the gel dries, the disappearance of the amorphous peak and an increase in the intensity of the peaks of the crystalline phase are observed, and a certain texturing of the sample associated with orientational crystallization on the silicon surface is also noticeable. Comparison of the observed diffraction peaks with the diffraction pattern simulated from single crystal data for sample (*R*)-**4** (Figure S1, curve 5) indicates that the nature of the formed xerogel corresponds to the enantiopure bulk crystalline phase.

Powder XRD results for compounds (R)-6.

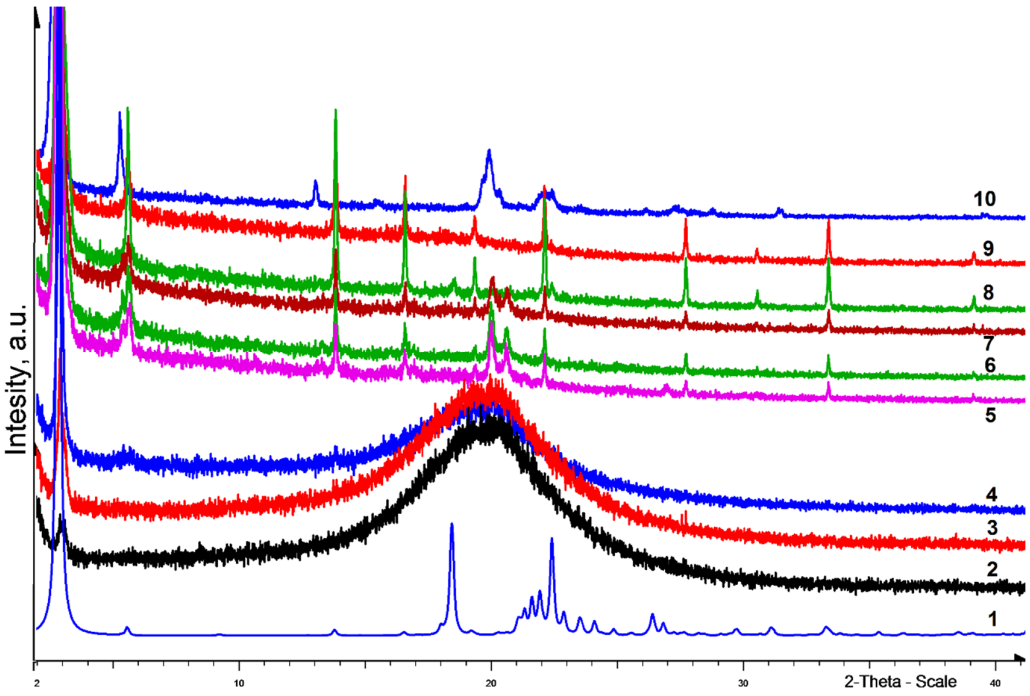

Figure S2. Powder diffraction patterns (bottom-up): (1) theoretical diffraction pattern calculated from single crystal data for (*R*)-**6** diol; (2–6) evolution of the diffraction of a gel based on (*R*)-**6** as the solvent naturally evaporates; (7) the dried gel is disordered on the surface of the silicon plate; (8) the sample is reloaded again to eliminate texture; (9) a drop of solvent is added to the sample; (10) experimental diffraction pattern of a polycrystalline enantiopure sample *rac*-**6**.

Diffraction patterns of the gel based on (*R*)-**6** sample (curves 2-4 in Figure S2) are typical for good gelling compounds and are characterized by almost no reflections of the crystalline phase, except for a broadened diffraction peak of low intensity in the region of diffraction angles of 3° in 2θ scale. As the sample turns into a xerogel, in addition to an increase in the intensity of the noted peak at 3°, the sets of reflections begin to appear in the angular ranges of 5-6, 13-14, and 20-21°. Comparison of the stabilized diffraction pattern with the diffractograms of enantiopure (curve 1, calculated from single crystal data) and polycrystalline racemic samples (curve 10) does not exclude the presence of an insignificant impurity of the racemate in the xerogel. Note that the diffraction peak in the range of diffraction angles of 3° in 2θ, corresponding to reflection from the family of basal planes (002), turns out to be close in magnitude for crystals of enantiopure and racemic samples; therefore, it is difficult to judge the belonging of this peak in the initial diffractogram, especially taking into account that the SC-XRD experiment was performed at low temperature (150K), while all PXRD experiments were performed at room conditions.

Powder XRD results for compounds (R)-7.

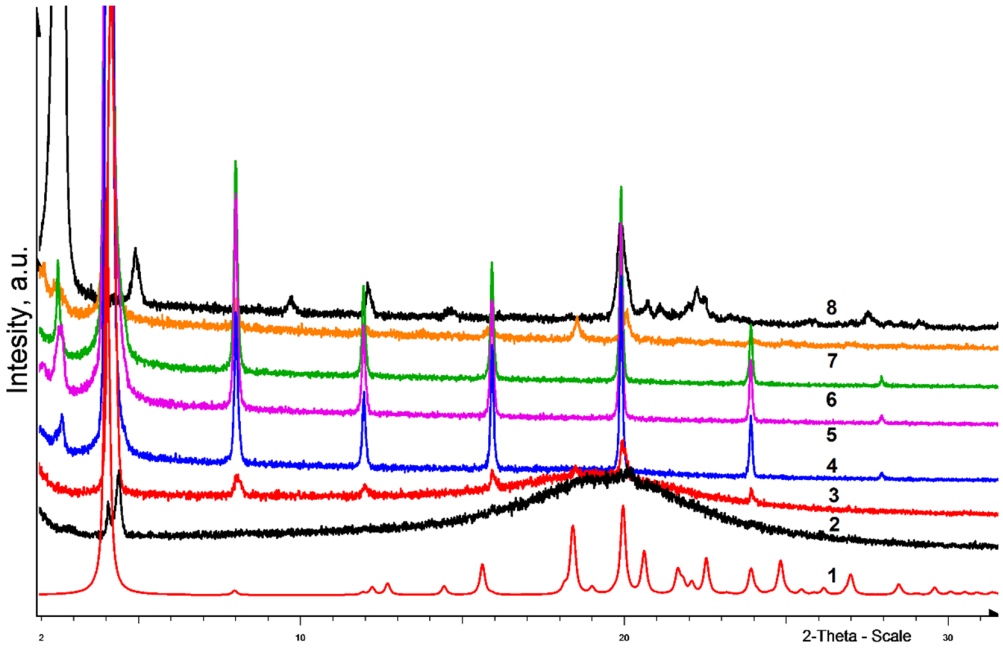

Figure S3. Powder diffraction patterns (bottom-up): (1) theoretical diffractogram calculated from single crystal data for diol (*R*)-**7**; (2-6) evolution of (*R*)-**7** based gel diffraction as the solvent naturally evaporates; (7) xerogel diffraction pattern after elimination of sample texturing; (8) experimental diffraction pattern of a *rac*-**7** polycrystalline sample.

On powder diffraction patterns of a gel based on heptyl derivative (*R*)-**7** with an enantiomeric excess about 98% (Figure S3), the presence of a xerogel can be observed already in the initial gel (curve 2). This is indicated by the presence of well-defined reflections in the range of angles 4-5° 2θ, corresponding to the enantiopure phase, and a weak shoulder in the range of angles 2.5°, characteristic of the basal reflex of the racemic phase (compare curve 8). As the sample dries (curves 3-6), strong texturing of the xerogel is observed; however, disordering and reloading of the sample (curve 7) make it possible to noticeably reduce this effect. Thus, the final product contains mainly the crystalline enantiopure phase (compare with curve 1 calculated from single crystal data) and traces of impurity crystals of the racemate (compare with the experimental diffractogram of the *rac*-**7** sample, curve 8).

Powder XRD results for compounds (R)-12.

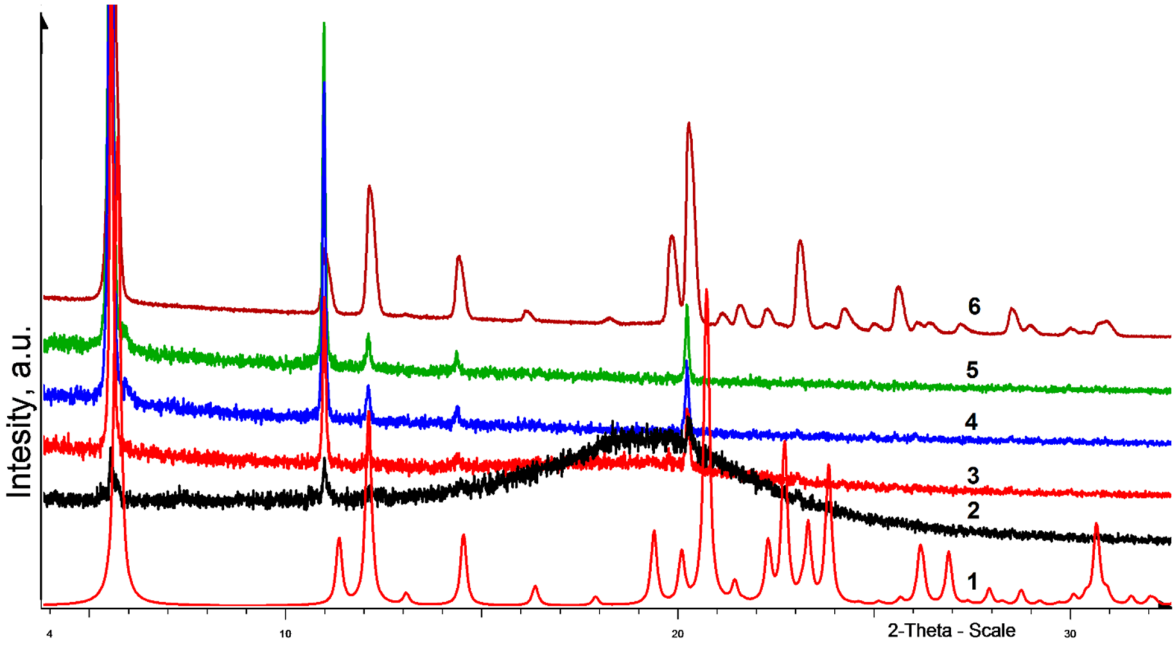

Figure S4. Powder diffraction patterns (bottom-up): (1) theoretical diffractogram calculated from single crystal data for diol *rac*-**12**; (2–5) evolution of (*R*)-**12** based gel diffraction as the solvent naturally evaporates; (6) experimental diffraction pattern of a polycrystalline enantiopure sample (*R*)-**12**.

In the initial diffraction pattern of the gel based on diol (*R*)-**12** (Figure S4), in addition to the amorphous halo, diffraction peaks are observed in the range of scattering angles 5-6, 10.5-11.5 and 20-21°, 2θ scale, indicating the presence of a crystalline phase (curve 2). As the gel dries, the disappearance of the amorphous halo is observed, accompanied by the appearance of additional diffraction peaks and an increase in the intensity of the initial peaks (curves 3-5). Comparison of the observed diffraction peaks with the experimental powder diffractogram of the enantiopure sample (curve 6) and the diffractogram simulated from single crystal data of the racemic sample (curve 1) allows us to conclude that the xerogel formed corresponds to the crystalline phase of the enantiopure sample.

Crystal-formative motifs for compound (R)-7.

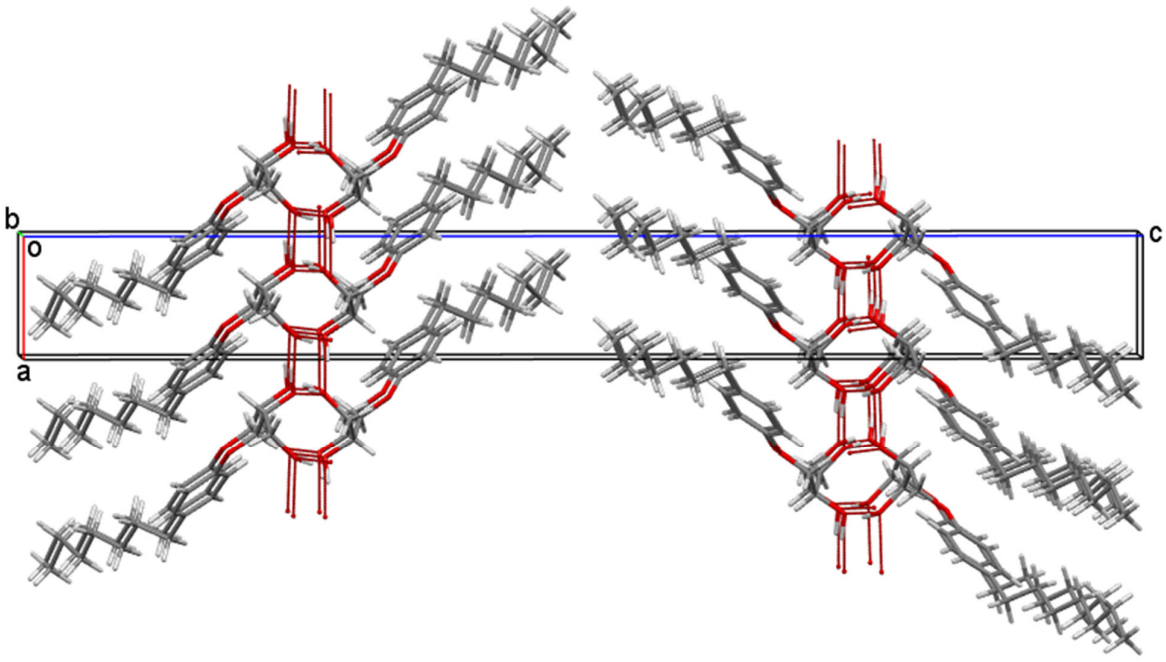

Figure S5. Fragment of (*R*)-**7** crystal packing; two BL-1 bilayers in the crystal cell. View along the axis *0b*.

Single crystals XRD results and crystal-forming motifs for compound (R)-8.

The octyl derivative (*R*)-**8** crystallizes in space group $P2_1$ with two independent molecules A and B in the asymmetric unit of the unit cell. The data in Table S3 indicate that these molecules (as well as molecules in (*R*)-**6** crystals) significantly differ in the conformation of their glycerol moieties in comparison between themselves or with the molecules (*R*)-**5** and (*R*)-**7**. These conformational differences are directly related to the different roles of these symmetrically independent molecules in the formation of supramolecular primary motif in the crystals of (*R*)-**8**. This crystal formative motif again appears a bilayer, as presented in Figure S6.

As in the case of guaifenesin-like packing, the bilayer is formed parallel to the plane *0ab*, and once again the basic interactions forming bilayer are classic IMHB O–H···O, which are concentrated in the central hydrophilic part, surrounded on both sides with hydrophobic hydrocarbon moieties. The central elements of the bilayer motif in the (*R*)-**8** crystals are again 1D spiral IMHB sequences formed around the screw axes 2_1 and developing along the *0b* direction. But in contrast to the case analyzed above, a full turn of such a spiral is formed with a participation of not 4, but 6 molecules, namely of four A molecules and of two B molecules.

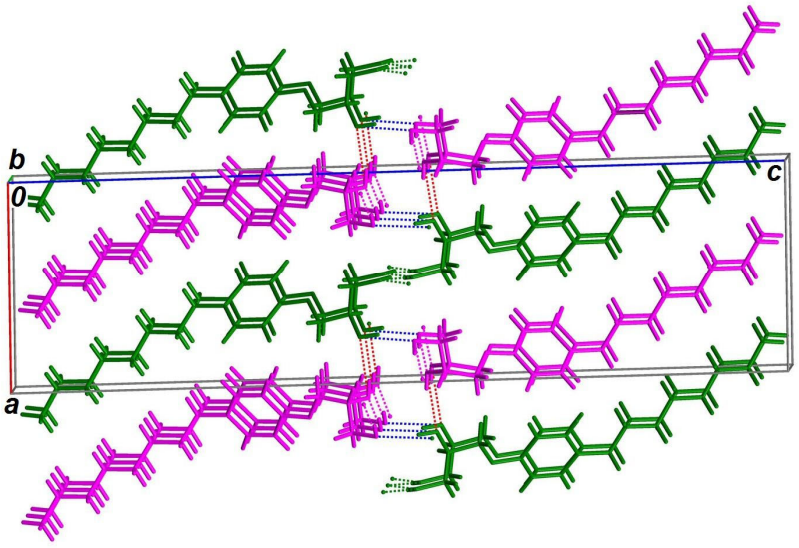

Figure S6. Fragment of (*R*)-**8** crystal packing; the independent A molecules are colored in magenta, the independent molecules B are colored in green. Colored dotted lines mark intermolecular hydrogen bonds. View along the axis *0b*.

As this takes place the molecules A provide to a helix construction both primary and secondary hydroxyls, whereas the molecules B provide only secondary hydroxyls O2–H2. A full turn of the helix (with a pitch equal to parameter *b* = 4.626 Å) is described by a sequence of six H-bonds: O2A–H2A···O2B–H2B···O1A'–H1A'···O2A''–H2A''···O2B'–H2B'···O1A–H1A···

{O2A'''–H2A'''···}. In Figure S7, this sequence is displayed by "spacefill" style; the figure clearly shows that within the (*R*)-**8** crystals the left *M*-helixes arise.

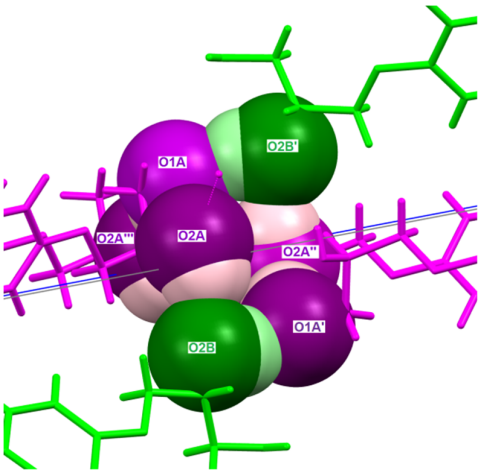

Figure S7. The spiral sequence of intermolecular hydrogen bonds in the (*R*)-**8** crystals.

Single crystals XRD results and crystal forming motifs for compound (R)-9.

Comparison of the characteristics of the unit cell for the ethers (*R*)-**8** and (*R*)-**9** (Table S2) shows that, while the space group $P2_1$ and two symmetry independent molecules are maintaining for both compounds, owing to elongation of alkyl substituent of one methylene unit, the character of the packing is changed again. Figure S8 shows a fragment of the crystal packing, which corresponds to the primary supramolecular motif in the (*R*)-**9** crystals. Shown in the figure 1D column is developed around the screw axis 2_1. These columns are formed by two pairwise symmetric systems of intermolecular H-bonds. One such system, which is designated by green dotted lines, represents a sequence of bifurcate intermolecular hydrogen bonds with the participation of secondary hydroxyl groups of B molecules, namely O2B–H2B···O3A [(x,1+y,z), ∠OHO = 138(9)°, d = 2.88(1) Å] and O2B–H2B···O2A [(x,1+y,z), ∠OHO = 139(9)°, d = 3.00(1) Å].

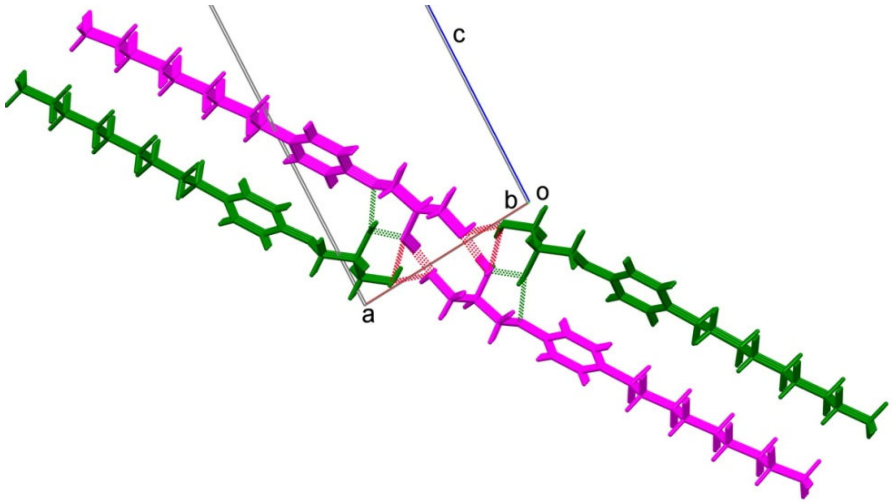

Figure S8. Detail of (*R*)-**9** crystal packing; independent A molecules are colored in magenta, independent B molecules are colored in green. Colour dotted lines mark intermolecular hydrogen bonds. View along the *0b* axis.

The primary hydroxyl of B molecules and both hydroxy groups of A molecules are involved in the formation of two axially symmetrical relative to each other helical sequences of IMHB allocated to Figure S8 by red dotted lines. A full turn of such a spiral is formed with the participation of three molecules through the sequence of hydrogen bonds O2A–H2A···O1A' [(-1-x,-1/2+y,-z), ∠OHO = 167(8)°, d = 2.66(1) Å], O1A'–H1A'···O1B [(-1-x,-1/2+y,-z), ∠OHO = 157(10)°, d = 2.73(1) Å] and O1B–H1B···O2A" [(x,1+y,z), ∠OHO = 162(10)°, d = 2.76(1) Å]. From Figure S9, in which one of these helixes is labeled by "spacefill" style, it is clear that it has the right-handed P-configuration.

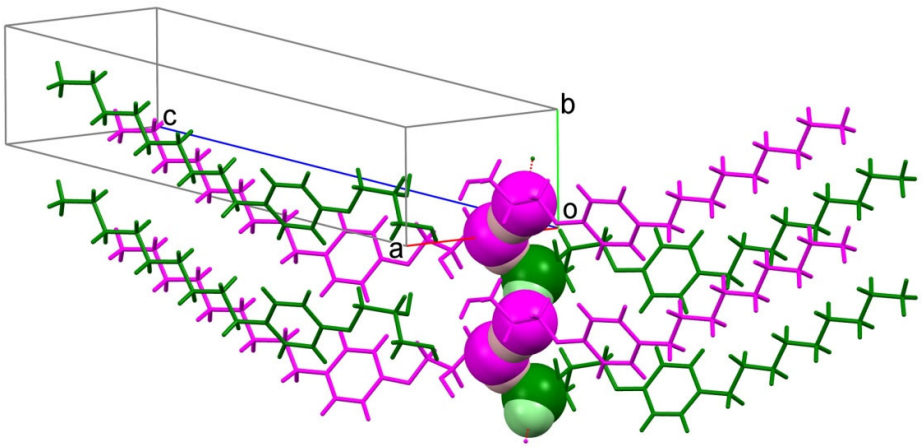

Figure S9. One of the right-handed spiral sequences of intermolecular hydrogen bonds in the (*R*)-**9** crystals.

Table S5. Solubility data[1] of some alkyl substituted phenyl glycerol ethers in cyclohexane (20°C).

Alkyl	No comp.	C_S, mmol L^{-1}
para-Me	*rac*-**1**	1.08 (0.20 mg mL^{-1})
	scal-**1**	1.46 (0.27 mg mL^{-1})
para-Et	*rac*-**2**	1.42 (0.28 mg mL^{-1})
	scal-**2**	2.09 (0.41 mg mL^{-1})
para-*n*Pr	*rac*-**3**[2]	1.55 (0.32 mg mL^{-1})
	scal-**3**	0.84 (0.17 mg mL^{-1})
para-*n*Bu	*rac*-**4**	2.48 (0.55 mg mL^{-1})
	scal-**4**	1.27 (0.28 mg mL^{-1})
ortho-Me	*rac*-**10**[2]	1.94 (0.35 mg mL^{-1})
	scal-**10**	1.00 (0.18 mg mL^{-1})
ortho-Et	*rac*-**12**[2]	3.70 (0.72 mg mL^{-1})
	scal-**12**	1.77 (0.35 mg mL^{-1})
meta-Me	*rac*-**13**	1.32 (0.24 mg mL^{-1})
	scal-**13**	1.89 (0.34 mg mL^{-1})
para-*n*Octyl	*scal*-**8**	< 1 (< 0.28 mg mL^{-1})[3]

[1.] – Solubility was determined using HPLC according to the method described in our work [1].
[2.]- The racemic compound crystallizes as a conglomerate.
[3.]- Determined by weight method.

References

1. Bredikhin, A.A.; Zakharychev, D.V.; Fayzullin, R.R.; Antonovich, O.A.; Pashagin, A.V.; Bredikhina, Z.A. Chiral *para*-alkyl phenyl ethers of glycerol: synthesis and testing of chirality driven crystallization, liquid crystal, and gelating properties. *Tetrahedron: Asymmetry* **2013**, *24*, 807–816. DOI: 10.1016/j.tetasy.2013.05.017